

# Real-time retrieval of precipitable water vapor from GPS and BeiDou observations

Cuixian Lu<sup>1</sup> · Xingxing Li<sup>1</sup> · Tobias Nilsson<sup>1</sup> · Tong Ning<sup>1</sup> · Robert Heinkelmann<sup>1</sup> · Maorong Ge<sup>1</sup> · Susanne Glaser<sup>2</sup> · Harald Schuh<sup>1</sup>

Received: 4 January 2015 / Accepted: 17 April 2015 / Published online: 28 April 2015  
© Springer-Verlag Berlin Heidelberg 2015

**Abstract** The rapid development of the Chinese BeiDou Navigation Satellite System (BDS) brings a promising prospect for the real-time retrieval of zenith tropospheric delays (ZTD) and precipitable water vapor (PWV), which is of great benefit for supporting the time-critical meteorological applications such as nowcasting or severe weather event monitoring. In this study, we develop a real-time ZTD/PWV processing method based on Global Positioning System (GPS) and BDS observations. The performance of ZTD and PWV derived from BDS observations using real-time precise point positioning (PPP) technique is carefully investigated. The contribution of combining BDS and GPS for ZTD/PWV retrieving is evaluated as well. GPS and BDS observations of a half-year period for 40 globally distributed stations from the International GNSS Service Multi-GNSS Experiment and BeiDou Experiment Tracking Network are processed. The results show that the real-time BDS-only ZTD series agree well with the GPS-only ZTD series in general: the RMS values are about 11–16 mm (about 2–3 mm in PWV). Furthermore, the real-time ZTD derived from GPS-only, BDS-only, and GPS/BDS combined solutions are compared with those derived from the Very Long Baseline Interferometry. The comparisons show that the BDS can contribute to real-time meteorological applications, slightly less accurately than GPS. More accurate and reliable water vapor estimates, about 1.3–1.8 mm in PWV, can be obtained if the BDS observations are combined with the GPS observations

in the real-time PPP data processing. The PWV comparisons with radiosondes further confirm the performance of BDS-derived real-time PWV and the benefit of adding BDS to standard GPS processing.

**Keywords** BeiDou · GPS · Precipitable water vapor · Tropospheric delay · Real-time precise point positioning · VLBI · Radiosonde

## 1 Introduction

Since Global Positioning System (GPS) meteorology was first proposed by [Bevis et al. \(1992\)](#) as an approach for sounding the atmospheric water vapor using ground-based GPS receivers; extensive investigations based on batch processing have been conducted in the past two decades ([Rocken et al. 1997](#); [Fang et al. 1998](#); [Gendt et al. 2004](#)). Various studies have proven that GPS could provide accurate water vapor estimates with an accuracy comparable to the measurements from meteorological sensors in post-processing and near-real-time modes ([Gendt et al. 2004](#)). Compared to the conventional water vapor observation systems such as radiosondes and water vapor radiometers, GPS displays several significant advantages including low operating cost, all-weather availability, and high spatio-temporal resolution.

Nowadays, the GPS-derived zenith total delays (ZTD) and precipitable water vapor (PWV) provide an important contribution to metrological applications. Tropospheric results of thousands of GPS stations are continuously generated and provided for assimilation into numerical weather prediction (NWP) models in near-real-time ([Dousa and Vaclavovic 2014](#)). As a notable example, in the European E-GVAP<sup>1</sup>

✉ Xingxing Li  
lxliq109121@gmail.com; lixin@gfz-potsdam.de

<sup>1</sup> German Research Centre for Geosciences GFZ, Telegrafenberg, 14473 Potsdam, Germany

<sup>2</sup> Technische Universitaet Berlin, Strasse des 17. Juni 135, 10623 Berlin, Germany

<sup>1</sup> <http://egvap.dmi.dk>.

project, more than 2400 continuously operating GPS stations are deployed to form a ground track network, providing near real-time PWV estimates for assimilation into NWP models. The establishment of several other projects and studies all demonstrated the ability of GPS serving as an accurate water vapor sensor for meteorological applications (Haan et al. 2004; Gutman et al. 2004; Elgered et al. 2005; Nilsson and Elgered 2008).

Many innovative applications such as nowcasting of severe weather events or regional short-term forecast systems could potentially benefit from more rapid updates of the atmospheric state. As addressed in the new European Earth System Science and Environmental Management (ESSEM) COST Action ES1206 “Advanced Global Navigation Satellite Systems Tropospheric Products for Monitoring Severe Weather Events and Climate (GNSS4SWEC)<sup>2</sup>”, it aims to exploit the full potential of Global Navigation Satellite Systems (GNSS) water vapor estimates for real-time monitoring and forecasting of severe weather events. The development and transition to real-time GNSS tropospheric products from the deferred-time mode has become one of the current topics within the GNSS meteorology community.

There are two data processing strategies for GNSS ZTD/PWV estimation: precise point positioning (PPP, Zumberge et al. 1997) and the baseline/network approach. The PPP approach is based on un-differenced (UD) observations and shows advantages concerning efficiency and flexibility compared to the baseline/network approach that incorporates double-differenced (DD) observations. Under the framework of the recent development of the International GNSS Service (IGS, Dow et al. 2009) real-time pilot project (RTPP), real-time precise satellite orbit and clock products are now available online (Caissy et al. 2012), which has greatly increased the interest in the real-time PPP technique (Li et al. 2011, 2013a). Therefore, PPP becomes a more promising tool for real-time GNSS ZTD/PWV retrieving and for supporting time-critical meteorological applications. Those developments are in accordance with the increasing demand of modern weather forecasting systems regarding higher temporal resolution for water vapor retrieval, especially for severe weather nowcasting (Li et al. 2014b; Dousa and Vaclavovic 2014; Yuan et al. 2014).

The Chinese BeiDou Navigation Satellite System (BDS) has been officially announced to provide continuous positioning, navigation, and timing (PNT) service since 2012, December 27, covering the whole Asia-Pacific region. The current BDS constellation consists of five Geostationary Earth Orbit (GEO), five Inclined Geo-Synchronous Orbit (IGSO), and four Medium Earth Orbit (MEO) satellites available for PNT services (China Satellite Navigation Office 2012). The installation phase for completing the constellation

with 5 GEO, 3 IGSO, and 27 MEO satellites is expected to be accomplished by the end of 2020. Based on the completion of the BDS regional system constellation and the establishment of several tracking networks, a number of investigations have been carried out recently related to the BDS precise orbit determination (POD), GPS/BDS combined POD, BDS precise point positioning, and relative positioning (Ge et al. 2012; Shi et al. 2012; Li et al. 2013a; Montenbruck et al. 2014). It has been demonstrated that BDS is capable of providing PNT service with an accuracy comparable to GPS (Ge et al. 2012; Li et al. 2015).

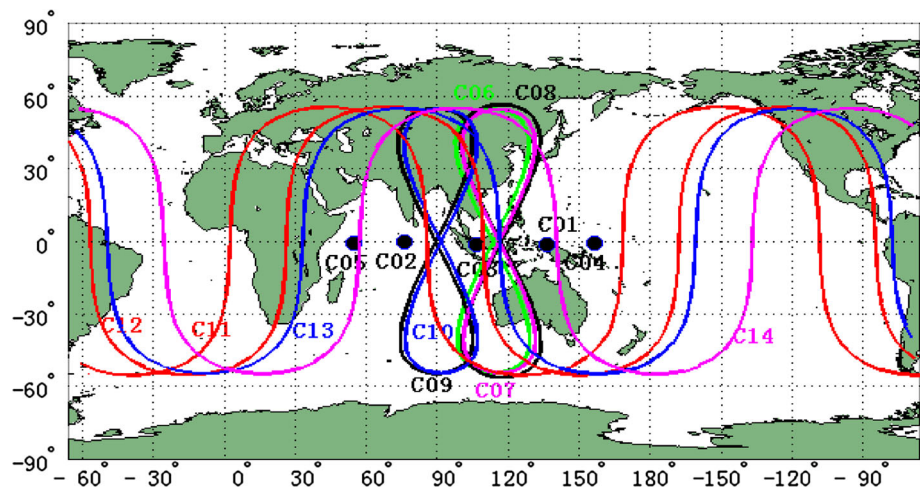
Xu et al. (2013) made an assessment on ZTD estimated from observations of a BDS local network with a time span of 4 days for the first time. Their comparison with GPS ZTD from IGS showed a bias and standard deviation of about 2 and 5 mm, respectively, being at the same level as the difference between GPS ZTD estimated by different software packages (Xu et al. 2013). According to the results from BeiDou Experiment Tracking Network (BETN), Li et al. (2014a) indicated that the PWV estimated from the BDS PPP can achieve similar precision as GPS-derived PWV. These initial results from post-processing are very promising, but it still needs further investigations and evaluations involving more globally distributed stations and longer time period, especially w.r.t. the performance of real-time water vapor retrieval from BDS. The addition of BDS to GPS significantly increases the number of observed satellites and optimizes the observation geometry accordingly. Thus, more slant total delays (STD) are available and more accurate and reliable ZTD/PWV estimates can be expected, which will provide a significant contribution to current GNSS meteorology (Bender et al. 2009).

In this contribution, we investigate the real-time water vapor retrieval from GPS and BDS observations. The observations from 40 globally distributed stations of the IGS Multi-GNSS Experiments (MGEX) and BETN are processed in real-time PPP mode to estimate ZTD/PWV. We assess the performance of real-time PWV retrieved from BDS data and evaluate the contribution of adding BDS to GPS for ZTD/PWV retrieval. Real-time ZTD derived from three different data sets: GPS-only, BDS-only, and GPS/BDS combined, are compared with those derived from the Very Long Baseline Interferometry (VLBI) technique for an independent reference at co-located GNSS/VLBI sites. The observations from nearby radiosondes are considered for inter-technique validation of the real-time PWV as well.

This article is organized as follows: we first describe the tracking network including MGEX and BETN, and the data sets for GPS, BDS, VLBI, and radiosondes in Sect. 2. In Section 3, the modeling of GPS/BDS ZTD/PWV is described, the real-time PPP processing strategies are illustrated in detail, and the processing strategies of VLBI and radiosonde data are introduced as well. Thereafter, the results of ZTD/PWV

<sup>2</sup> [http://www.cost.eu/COST\\_Actions/essem/Actions/ES1206](http://www.cost.eu/COST_Actions/essem/Actions/ES1206).

**Fig. 1** 24-h ground tracks of the current BeiDou satellites. C01–C14 are the pseudorandom noise (PRN) codes for BeiDou satellites



comparisons of GPS-only, BDS-only and combined solutions, and the inter-technique validations with VLBI- and radiosonde-derived ZTD/PWV are presented in Sect. 4, followed by the conclusions in Sect. 5.

## 2 Tracking network and data collection

### 2.1 BDS and GPS data collection

After an effort of more than one decade, the BDS has been established independently (Ran 2010). Currently, it is foreseen to become an operational global navigation satellite system by 2020 according to a two-phase schedule. The first phase—completed by the end of 2012—includes five satellites in GEO at an altitude of 35,786 km, five in IGSO at an altitude of 35,786 km as well as with  $55^\circ$  inclination to the equatorial plane, and four in MEO at an altitude of 21,528 km and  $55^\circ$  inclination to the equatorial plane (Yang et al. 2011). The regional positioning and navigation services are operationally available for customers in the Asia-Pacific region. The 24-h ground tracks of the current BeiDou satellites are shown in Fig. 1.

The BETN established by Wuhan University<sup>3</sup> is a continuous global observation reference network. Since 2011 nine tracking stations in China and seven tracking stations outside of China have been included in BETN (Shi et al. 2012). Among them, the stations in China are BJF1 in Beijing, CENT in Wuhan, CHDU in Chengdu, HRBN in Harbin, HKTU in Hong Kong, NTSC and XIAN in Xi'an, SHAO in Shanghai, and LASA in Tibet. The seven non-Chinese stations are SIGP (Singapore), PETH (Australia), DHAB (United Arab Emirates), LEID (The Netherlands), JOHA (South Africa), PFTP (Australia), and XILA (Greece). All the stations are equipped with the UB240-CORS GPS/BDS

dual-system receivers and the UA240 antennas manufactured by the UNICORE Company,<sup>4</sup> China.

The MGEX campaign<sup>5</sup> was initialized by the IGS enabling a multi-GNSS service to track, collect, and analyze data from GPS, GLONASS, BeiDou, Galileo, Quasi-Zenith Satellite System (QZSS), and any space-based augmentation system (SBAS) of interest. Over the past 2 years, a new network of multi-GNSS monitoring stations within the domain of MGEX has been deployed around the world. Today, more than 100 stations are included in the MGEX network with excellent capability of multi-GNSS constellation tracking. Around 30 stations among them are capable of both, GPS and BDS, observations (Montenbruck et al. 2014).

In this study, GPS and BDS observations during the first half year of 2014 of about 40 stations from the BETN and MGEX network are processed in real-time PPP mode for ZTD/PWV estimation. The distribution of the stations, that can track GPS and BDS satellites, is shown in Fig. 2.

### 2.2 VLBI data

The VLBI technique is capable of determining accurate tropospheric delays as well as water vapor content in the vicinity of the VLBI stations (Schuh and Behrend 2012). Due to the similar observing mode and processing strategy of tropospheric parameters of VLBI and GNSS, the tropospheric zenith delays derived from VLBI are of great interest for the validation and calibration of parameters retrieved by GNSS (Heinkelmann et al. 2007; Teke et al. 2011; Ning et al. 2012). In this study, the VLBI is used as an independent technique to validate the real-time ZTD estimates derived from GPS and BDS observations. The VLBI observations during the latest CONT campaign (CONT14<sup>6</sup>) are used here.

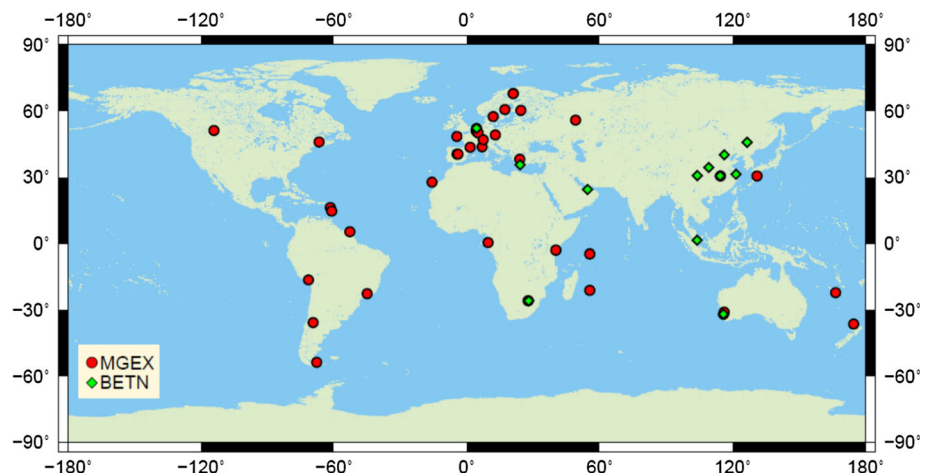
<sup>4</sup> <http://www.unicorecomm.com/english/>.

<sup>5</sup> <http://igs.org/mgex/>.

<sup>6</sup> <http://ivs.nict.go.jp/mirror/program/cont14/>.

<sup>3</sup> <http://en.whu.edu.cn/>.

**Fig. 2** The distribution of the GPS/BDS stations from BETN and MGEX



As a follow-on to the previous campaigns (CONT94, CONT95, CONT02, CONT05, CONT08, and CONT11), CONT14 is a special campaign of the International VLBI Service for Geodesy and Astrometry (IVS). The aim of CONT14 is to acquire state-of-the-art VLBI data over a time period of two weeks to demonstrate geodetic results of the highest accuracy the current VLBI system is capable of. CONT14 comprises a 15-day continuous VLBI observation campaign during the period 2014, May 6–20, with a network size of 17 stations (ten in the northern and seven in the southern hemisphere). Among these VLBI stations, Onsala60 (Onsala, Sweden) and Wark12m (Warkworth, New Zealand) are co-located with MGEX stations: ONS1 and WARK, respectively. Continuous VLBI observations are available at these two stations during CONT14 and will be employed for an independent comparison and validation of GPS- and BDS-derived ZTD. The horizontal distance of Onsala60 from the GNSS station ONS1 is within 200 m and the height difference between the VLBI antenna reference point and the GNSS antenna reference point is about 15 m. For Wark12m and WARK, the horizontal distance is within 100 m and the height difference is about 17 m.

### 2.3 Radiosonde data

Radiosondes (RS) are balloon-borne instruments that measure temperature, pressure, and humidity along the line of the sounding to the ground station using radio signals. The radiosonde profiles provide atmosphere information up to an altitude of approximately 30 km. The radiosonde balloons are released every 12 or 24 h per day in most cases. As one of the most reliable in-situ measurements of water vapor (Rocken et al. 1997), the radiosonde-measured water vapor is taken as another independent reference for validation of the GPS/BDS derived PWV. For the GPS/BDS observing network under investigation here, several stations are taken into account where nearby radiosonde observations (within 50

km) are available. The radiosonde data are accessible through their atmosphere profiles provided by the National Ocean and Atmospheric Administration<sup>7</sup> (NOAA).

## 3 Observation model and processing strategy

### 3.1 Real-time ZTD/PWV retrieval from GPS and BDS

Generally, the ionosphere-free combination of dual-frequency carrier-phase and pseudo-range (LC, PC) are utilized in PPP processing to eliminate the first-order effects of the ionosphere. The observation equation can be expressed as following: (Kouba 2009),

$$L = \rho + c(dt_r - dt_s) + T + B + \varepsilon_L \quad (1)$$

$$P = \rho + c(dt_r - dt_s) + T + \varepsilon_P, \quad (2)$$

where  $L$  and  $P$  are the ionosphere-free combination of carrier phase and pseudo-range,  $\rho$  is the geometric distance,  $dt_r$  and  $dt_s$  denote the receiver and satellite clock biases,  $c$  is the speed of light in vacuum,  $T$  is the tropospheric delay,  $B$  is the unknown phase ambiguity, and  $\varepsilon_L$  and  $\varepsilon_P$  denote the measurement noise and multipath error for carrier phase and pseudorange, respectively. The first order of ionospheric delay is eliminated by ionosphere-free linear combination; the phase center offset and variation, phase wind-up, tidal loading, Earth rotation, and relativistic effects can be corrected according to existing models (Kouba 2009). In the GPS/BDS combined data processing, inter-system biases (ISB) between GPS and BDS must be taken into account and the combined observation model can be expressed as follows:

<sup>7</sup> <http://www.esrl.noaa.gov/raobs/>.

$$\begin{cases} L^G = \rho^G + c(dt_r - dt_s^G) + T^G + B^G + \varepsilon_L^G \\ L^C = \rho^C + c(dt_r - dt_s^C) + ISB_L^{C-G} + T^C + B^C + \varepsilon_L^C \end{cases} \quad (3)$$

$$\begin{cases} P^G = \rho^G + c(dt_r - dt_s^G) + T^G + \varepsilon_P^G \\ P^C = \rho^C + c(dt_r - dt_s^C) + ISB_P^{C-G} + T^C + \varepsilon_P^C, \end{cases} \quad (4)$$

where the indices  $G$  and  $C$  refer to the GPS and BDS satellite systems;  $ISB_L^{C-G}$  and  $ISB_P^{C-G}$  denote the receiver internal biases (i.e. ISB) between GPS and BDS for carrier phase and pseudo-range, respectively. We set-up the code bias parameters for both GPS and BDS, but the code bias for GPS is set to zero to eliminate the singularity between receiver clock and code bias parameters. Consequently, the estimated biases of BDS are relative to the biases for GPS satellites. It is worthwhile to notice that such a receiver internal bias is only relevant for processing the code data. When analyzing the phase measurements, the corresponding phase ambiguity parameters will absorb the phase delays.

The tropospheric delay  $T$  consists of hydrostatic and non-hydrostatic/wet components. Both can be expressed by their individual zenith delays, gradients, and mapping functions:

$$T = m_{f_h} \cdot Z_h + m_{f_w} \cdot Z_w + m_{f_w} \cdot \cot(e) \cdot (G_N \cdot \cos(a) + G_E \cdot \sin(a)), \quad (5)$$

where  $Z_h$  and  $Z_w$  denote the zenith hydrostatic delays (ZHD) and zenith wet delays (ZWD), respectively,  $m_{f_h}$  and  $m_{f_w}$  represent the hydrostatic and wet mapping functions [here Global Mapping Functions (GMF), Böhm et al. (2006)],  $G_N$  and  $G_E$  are the horizontal north and east gradients, and  $e$  and  $a$  are the elevation and azimuth angles. ZHD accounts for about 90 % of the total tropospheric delay and ZWD for the remaining about 10 % (Davis et al. 1985). ZHD can be calculated with sufficient accuracy using empirical models such as the Saastamoinen equations (Saastamoinen 1973) with given surface pressure data. It is difficult to model ZWD with enough accuracy due to its very low mixing ratio with dry atmospheric constituents, its variability, and its sensitivity to weather conditions caused by atmosphere water vapor distribution. Thus, ZWD is usually modeled as an unknown parameter and estimated in the adjustment together with the other parameters.

In the real-time PPP ZTD/PWV processing, first of all precise satellite orbits and clocks are determined using data of a global GNSS ground tracking network. Similar to the procedure of the IGS ultra-rapid orbits, the real-time orbit is predicted (here 6 h prediction) based on the orbits determined in a batch-processing mode. Then, with fixed satellite orbits and station coordinates, satellite clocks are estimated and updated epoch-wise due to their short-term fluctuations. With these real-time orbit/clock corrections and precise station coordinates, the estimated parameter vector  $\mathbf{X}$  can be expressed as follows:

$$\mathbf{X} = (Z_w G_N G_E dt ISB_P^{C-G} B)^T \quad (6)$$

A sequential least squares filter is employed to estimate the unknown parameters in real-time processing (Li et al. 2013b). The tropospheric zenith wet delays  $Z_w$  and the north and east gradients  $G_N$  and  $G_E$  are modeled as random walk processes. The noise intensity of the quantity of greatest interest,  $Z_w$ , is about 5–10 mm/ $\sqrt{h}$ . The receiver clock bias  $dt$  is modeled as white noise and estimated epoch-wise. The code ISB between GPS and BDS,  $ISB_P^{C-G}$ , are assumed as constant over time and estimated as well. As mentioned above, the phase bias will be absorbed by the phase ambiguity  $B$ , and the ambiguity parameters are assumed constant and estimated during each continuous arc. An elevation-dependent weighting strategy is applied. Details of the GPS/BDS observation model and the data processing strategy are summarized in Table 1. The EPOS-RT software (Ge et al. 2012; Li et al. 2013c) is used for data processing in this work.

**Table 1** Observation model and data processing strategies for real-time ZTD/PWV retrieval from GPS and BDS

	GPS and BDS processing
Observations	Undifferenced ionosphere-free phase and pseudo-range combinations
Estimator	Sequential least squares filter
Frequency	GPS: L1, L2; BDS: B1, B2
Elevation cutoff	5°
Sampling rate	30 s
Weighting strategy	Elevation-dependent weighting; 2 mm for phase raw observables and 0.6 m for code raw observables for both GPS and BDS
Satellite orbit and clock	Fixed, predicted orbit and epoch-wise clock
Zenith tropospheric delay	Saastamoinen model + random walk process
Tropospheric gradients	Estimated
Mapping function	Global Mapping Function (GMF)
Phase wind-up	Applied
Station displacement	Solid Earth tide, ocean tide loading, pole tide
Receiver clock bias	Estimated as white noise
Station coordinates	Fixed
Inter-system bias	Estimated as constant
Satellite antenna PCO and PCV	Corrected using IGS and MGEX values
Receiver antenna PCO and PCV	Corrected
Ionospheric delay	Eliminated by ionosphere-free combination

Once  $Z_w$  is accurately estimated, it can be directly related to PWV (Askne and Nordius 1987) by

$$\text{PWV} = \prod(T_m) \cdot Z_w, \quad (7)$$

where the parameter  $\prod(T_m)$  varies as a function of the weighted mean temperature of the atmosphere  $T_m$  (Bevis et al. 1992):

$$\prod(T_m) = \frac{10^6}{\rho_w R_v \left( \frac{k_3}{T_m} + k_2' \right)}, \quad (8)$$

where  $\rho_w = 999.97 \text{ kg m}^{-3}$  denotes the density of liquid water,  $R_v = 461.51 \text{ J K}^{-1} \text{ kg}^{-1}$  is the specific gas constant of water vapor,  $k_3$  and  $k_2'$  are atmospheric refraction constants:  $k_2' = 22.1 \pm 2.2 \text{ (K hpa}^{-1}\text{)}$ ,  $k_3 = 373,900 \pm 1200 \text{ (K}^2 \text{ hpa}^{-1}\text{)}$ . To calculate  $T_m$ , vertical profiles of water vapor and temperature are required (Davis et al. 1985). It was shown that  $T_m$  can be well obtained from the global reanalysis of the European Centre for Medium-Range Weather Forecasts (ECMWF). The difference between  $T_m$  from ECMWF and from global radiosonde observations is less than 2 K for most of the stations (Wang et al. 2005). Thus, in this study,  $T_m$  from ECMWF reanalysis (ERA-Interim<sup>8</sup>) are used for the conversion from ZWD into PWV.

If the a priori ZHD is not calculated accurately, the error will be absorbed by the estimated ZWD during parameter estimation and consequently propagate to the PWV. Accurate modeling of ZHD requires the availability of surface pressure values that can be obtained from meteorological sensors, from NWP models, from empirical models, or from other sources. Therefore, in a first step the Global Pressure and Temperature 2 model (GPT2, Lagler et al. 2013) is applied to obtain the a priori ZHD, and consequently the PPP-derived ZTD. Thereafter, more accurate ZHD are calculated with the meteorological data from ERA-Interim reanalysis of ECMWF interpolated at the position of each GNSS antenna. Accurate ZWD are then generated from the PPP-derived ZTD by subtracting the more accurate ZHD and finally, the accurate ZWD is converted into PWV following Eq. (7).

### 3.2 VLBI data processing

In a single VLBI observation an extragalactic radio source, e.g. a quasar, is observed in parallel with two radio telescopes (Schuh and Behrend 2012). The observed delay is the difference in time of arrival of the noise from the radio source at the two stations. The ionosphere free delay can be expressed as

$$\tau = -\vec{b}^T Q \vec{k} + T_1 - T_2 + dt_1 - dt_2, \quad (9)$$

<sup>8</sup> [http://apps.ecmwf.int/datasets/data/interim\\_land/](http://apps.ecmwf.int/datasets/data/interim_land/).

where  $\vec{b}$  is the baseline vector between the stations,  $\vec{k}$  denotes the unit vector in the direction of the radio source, the matrix  $Q$  represents the orientational part of the transformation between the celestial and the terrestrial reference systems (Petit and Luzum 2010),  $T_i$  are the tropospheric delays at station  $i = 1, 2$ , and  $dt_i$  represent the clock errors of station  $i$ . Just as for the GNSS processing, the tropospheric delay can be described by Eq. (5).

Here, the VLBI data were analyzed using the GFZ version of the Vienna VLBI Software (Böhm et al. 2012), VieVS@GFZ. This software estimates the unknown parameters in a classical least squares adjustment. The estimated parameters include clock corrections, ZWD, Earth orientation parameters (EOP), and horizontal gradients. The ZHD were modeled using the Saastamoinen model (Saastamoinen 1973) with meteorological data from GPT2, which is consistent with the modeling of the a priori ZHD in GNSS data processing. The ZWD were parameterized as piece-wise linear functions with interval length of 1 h and the gradients were estimated with interval length of 6 h. The GMF were used as the hydrostatic and wet mapping functions. In addition, we also estimated session-wise values of radio source coordinates, and all five EOP (polar motion, UT1-UTC, celestial pole offsets). The a priori and other models used in the analysis are listed in Table 2.

### 3.3 Radiosonde data processing

The observation profiles derived from radiosonde data are discrete series of temperature and relative humidity observations at different heights above the radiosonde launch site, which separates the atmosphere into several layers. Assuming linear water vapor density variation for each layer, the PWV along the path of the sounding balloon can be calculated by (Bevis et al. 1992),

$$\text{PWV} = \frac{1}{\rho_w} \sum (h_{i+1} - h_i) \cdot (\rho_v^{i+1} + \rho_v^i)/2, \quad (10)$$

where the variable  $\rho_v$  denotes the density of water vapor,  $\rho_w$  is the density of liquid water, the super- and subscripts  $i + 1$  and  $i$  denote the top and bottom of each layer for height and water vapor density. The water vapor density  $\rho_v$  can be calculated with temperature and relative humidity.

## 4 Results and analysis

### 4.1 Real-time ZTD derived from BDS, GPS and GPS/BDS combined solutions

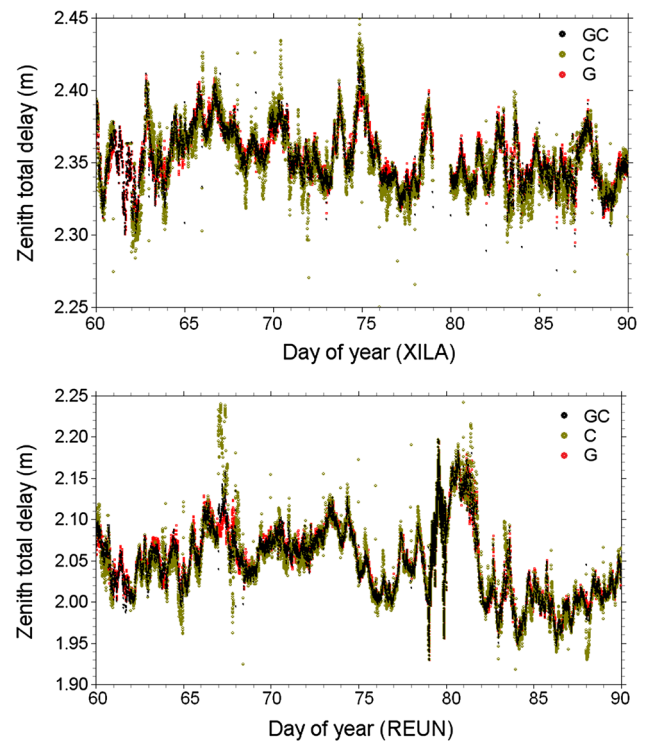
In order to assess the performance of the real-time BDS ZTD/PWV processing and also evaluate the contribution of

**Table 2** Observation model and data processing strategies for ZTD retrieving from VLBI

	VLBI processing
Observations	Ionosphere-free group delays
Estimator	Classical least squares
Frequency	X-band (8.4 GHz) and S-band (2.3 GHz)
Elevation cutoff	5°
Weighting strategy	The formal errors from the correlator plus a noise floor of 1 cm
Zenith tropospheric delay	Saastamoinen model + piece-wise linear function (1 h interval)
Tropospheric gradients	Estimated, piece-wise linear function (6 h interval)
Pressure and temperature	GPT2
Mapping function	GMF
Precession/nutation model	IAU2006/2000A
Earth rotation parameter	Estimated as daily offsets
Sub-diurnal EOP	IERS Conventions ( <a href="#">Petit and Luzum 2010</a> )
Station displacement	Solid Earth tide, ocean tide loading, pole tide, ocean pole tide, non-tidal atmospheric loading, VLBI antenna thermal deformation ( <a href="#">Nothnagel 2009</a> )
Receiver clock	Piece-wise linear function (1 h interval)
Radio source coordinates	Estimated, NNR w.r.t. ICRF2
Ionospheric delay	Eliminated by first-order ionosphere correction

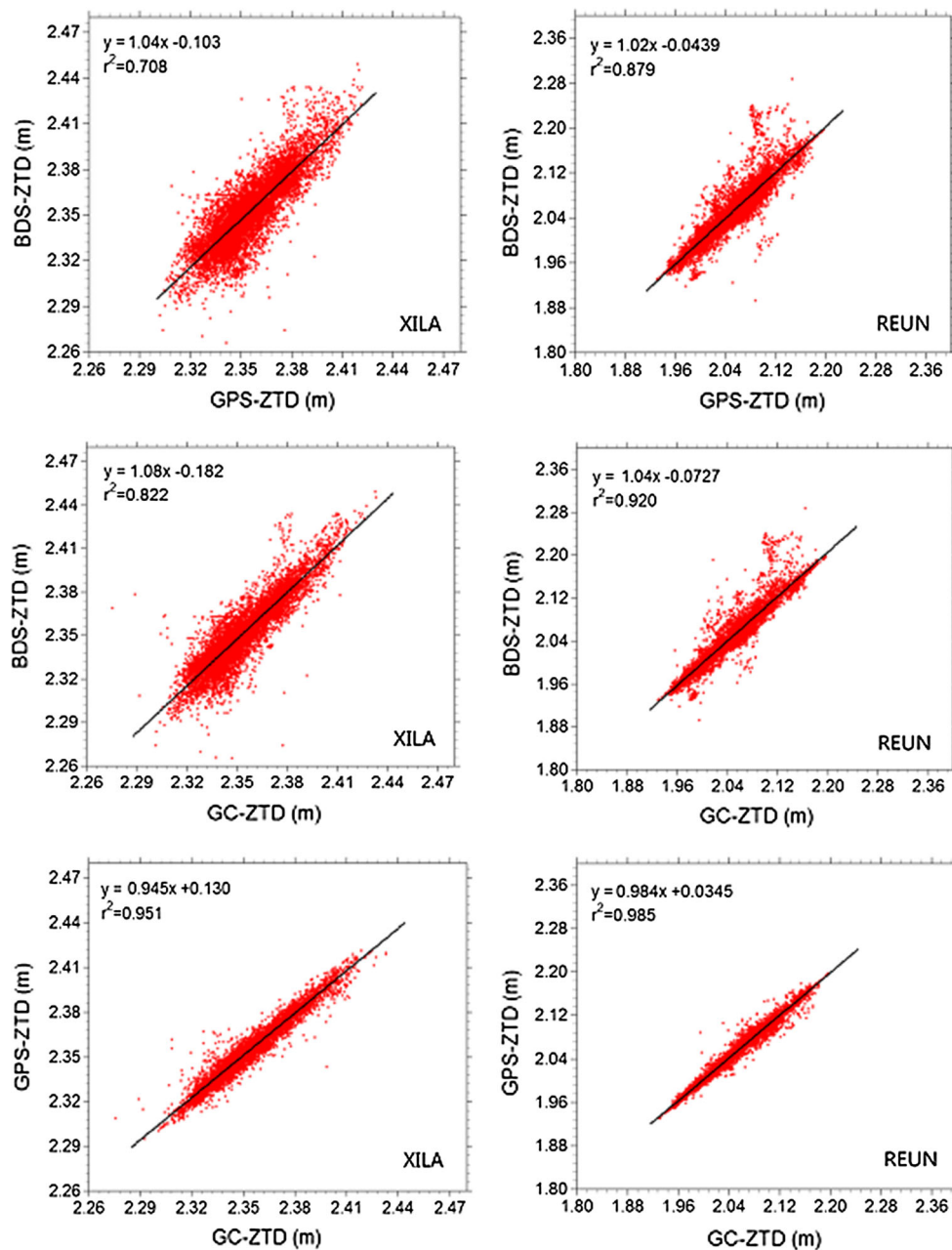
adding BDS to GPS for ZTD/PWV retrieval, we processed about 40 stations from the BETN and MGEX networks for the period of the first half of the year 2014. These stations have been selected because the BDS and GPS observations are available simultaneously. The GPS-only, BDS-only, and GPS/BDS combined PPP solutions are carried out to derive the corresponding ZTD/PWV estimates. All the data are processed in real-time PPP mode with a 30-s sampling interval to generate ZTD/PWV following the description in Sect. 3.1. The station coordinates are fixed to weekly solutions. The precise orbit and clock products applied are those generated in simulated real-time mode from about 130 globally distributed stations selected from IGS, MGEX, and BETN networks.

Figure 3 shows the ZTD time series of two stations during March 2014 as examples: XILA (35.53°N, 24.07°E, 177.79 m), Greece; and REUN (21.21°S, 55.57°E, 1558.40 m), island of Réunion, Indian Ocean east of Madagascar. The GPS-only and BDS-only ZTD are displayed by red and



**Fig. 3** ZTD derived from GPS-only (“G”), BDS-only (“C”), and GPS/BDS (“GC”) combined real-time PPP solutions at stations XILA (top) and REUN (bottom) for day of year (DOY) = 60–90, i.e. about March 2014

olive symbols, while the ZTD derived from the GPS/BDS combined solution are illustrated by black symbols. It can be noticed that the BDS-only ZTD derived from real-time PPP agree well with the GPS-only ZTD in general; however, they exhibit more outliers and larger noise. Possible reasons may be the signal instability or the low precision of the error models for BDS (e.g. the PCO and PCV model) since they are developed well for GPS ([Wang et al. 2014](#)). One can also see that the GPS/BDS combined ZTD agree better with the GPS-only solution than with the BDS-only solution. Some outliers of the GPS-only solution disappear when both, GPS and BDS, observations are combined together. The ZTD time series estimated from the GPS/BDS combined solution are more robust and smoother than the individual solutions. The addition of BDS to GPS can improve the quality of ZTD estimates because of the larger number of satellites and the improved observation geometry. For example, about 3–7 BeiDou and 6–10 GPS satellites are used, respectively, in the BDS- and GPS-only solution at the station XILA, while all the available BDS and GPS satellites (10–16 satellites) are used in the GPS/BDS combined solution. Figure 4 depicts the linear correlation between these three solutions at stations XILA and REUN. It can be noticed that the BDS ZTD and GPS ZTD are highly correlated; the correlation coefficients are 0.84 and 0.94 at the stations XILA and REUN,



**Fig. 4** Correlation of ZTD between BDS-only and GPS-only solutions, BDS-only and the combined solutions ("GC"), GPS-only and the combined solutions at stations XILA (*left*) and REUN (*right*)

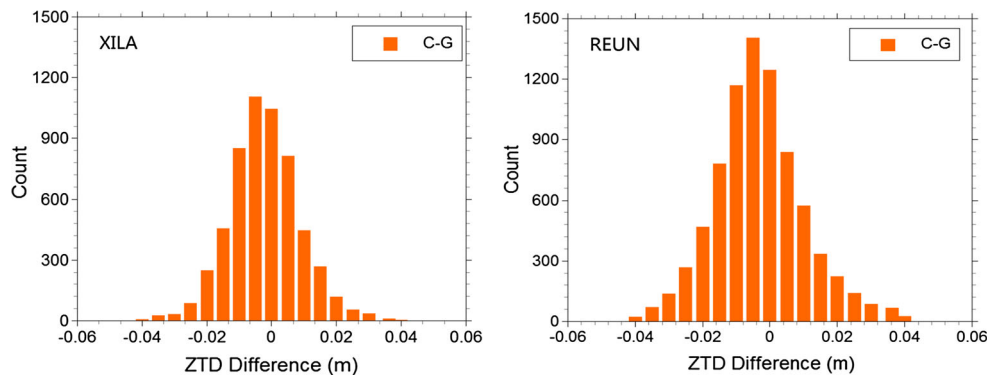
respectively. The correlation coefficients between the BDS ZTD and the combined ZTD are 0.91 and 0.96, while correlation coefficients between the GPS ZTD and the combined ZTD are 0.97 and 0.99 at the two stations.

Figure 5 presents the distribution of ZTD differences between BDS-only and GPS-only solutions at the abovementioned stations XILA and REUN during the same period. As can be noticed, the frequency count of the ZTD differences is close to normal distribution. The root mean square (RMS) values of the ZTD differences at the two stations are 11.0

and 11.9 mm, respectively, showing agreement at the level of about 1 cm. The mean values of the differences between BDS- and GPS-derived ZTD at the two stations are  $-2.2$  and  $-2.6$  mm, and their standard deviation (STD) values are 10.8 and 11.7 mm, respectively.

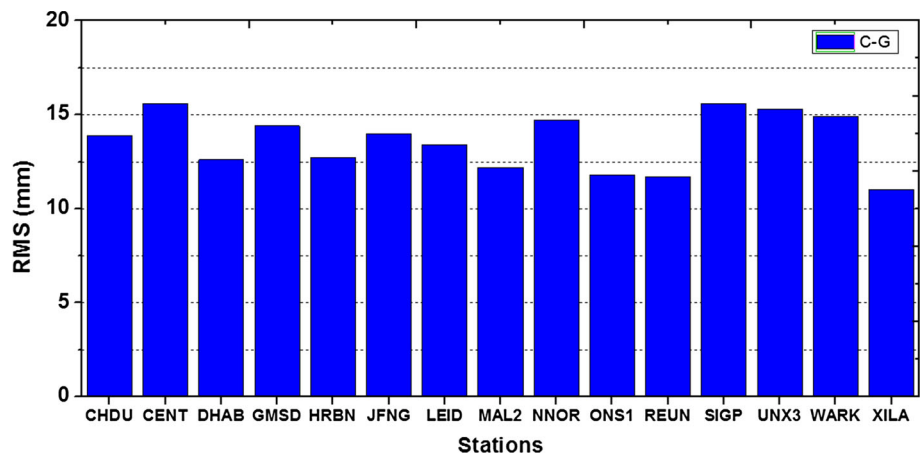
In Fig. 6, the statistical results of ZTD differences between BDS-only and GPS-only solutions are shown for 15 globally distributed stations. Those stations observe more than four BDS satellites and have good and continuous data during the processing period. The RMS values of the ZTD differences





**Fig. 5** Distribution of ZTD differences between BDS-only and GPS-only solutions derived from real-time PPP at stations XILA (*left*) and REUN (*right*) for day of year (DOY) = 60–90, i.e. about March 2014

**Fig. 6** RMS values of the ZTD differences between BDS-only and GPS-only solutions



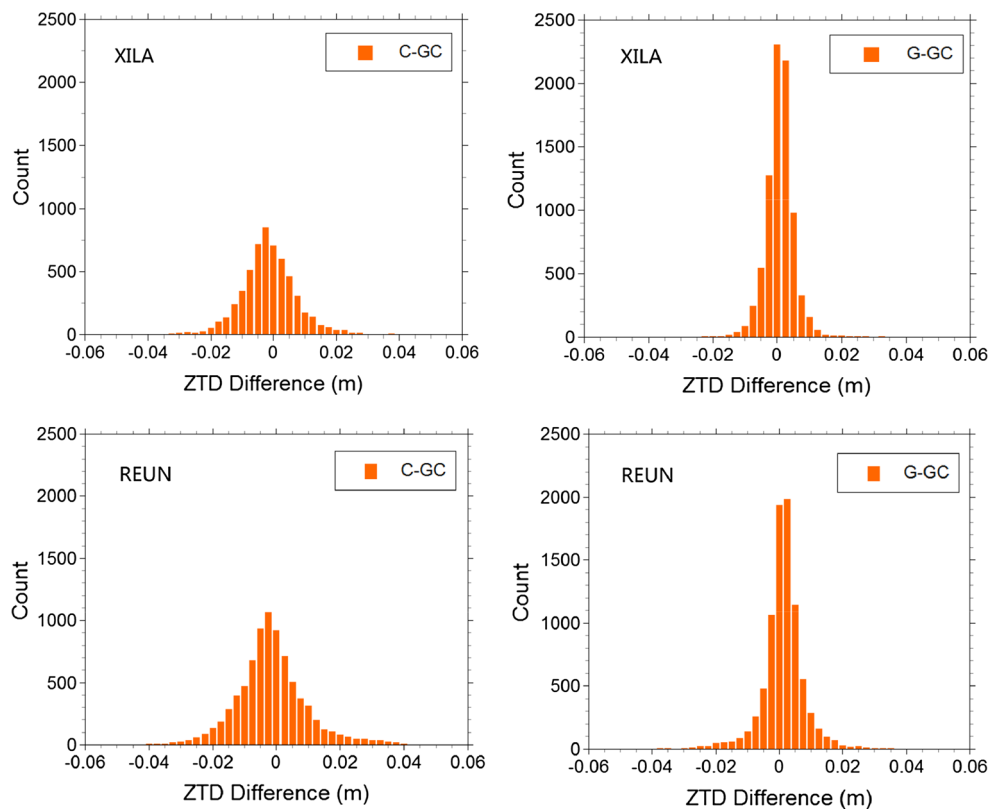
are 11–16 mm (which equals 2–3 mm in PWV), and the mean values of the differences are at the level of a few millimeters (usually smaller than 1 mm in PWV). The averaged RMS value of all the stations is 13.1 mm. This agreement implies that the real-time ZTD/PWV estimates from BDS observations only can significantly contribute to weather nowcasting, although their accuracy is slightly worse than that of the GPS-only solution [about 1.5 mm in PWV; Li et al. (2014b)]. At the moment the reliability of real-time BDS ZTD/PWV is not as good as that of GPS, especially out of the Asia-Pacific region. However, this situation will improve once the BDS constellation is complete.

Figure 7 shows the distribution of ZTD differences of BDS-only and GPS-only solutions with respect to the GPS/BDS combined solution. As displayed, the differences for the BDS ZTD mainly locate within the domain of –15 to 15 mm, while those for the GPS ZTD mainly range from –10 to 10 mm. The frequency count of the ZTD differences for both solutions behaviors as normal distribution. It is obvious that the ZTD differences for the GPS-only solutions are smaller than those of the BDS-only solutions on average. The differences between the BDS and combined solutions are about a few millimeters and show larger noise and a larger

number of outliers. The mean values of the differences for GPS ZTD are 0.7 and 0.9 mm at the two stations, and the mean values of the differences for BDS ZTD are –1.5 and –0.6 mm, respectively. The RMS values are 4.4 and 4.9 mm for GPS ZTD, and 8.5 and 9.6 mm for BDS ZTD. It is notable that both GPS and BDS ZTD show a good agreement with the combined solution, while the GPS results show smaller RMS and mean values than the BDS results.

#### 4.2 Inter-technique ZTD validation: GNSS vs. VLBI

For the sake of an independent inter-technique validation, the GNSS ZTD series retrieved from real-time PPP processing are compared with those from co-located VLBI stations. Figure 8 shows the ZTD comparisons of GPS-only, BDS-only, GPS/BDS combined and VLBI solutions at the multi-GNSS stations ONS1 (co-located with VLBI station ONSALA60), and WARK (co-located with VLBI station WARK12M). Here, the ZTD estimates over the 15-day CONT14 campaign are compared due to the availability of continuous VLBI observations during this period. These VLBI data are processed for ZTD derivation following the



**Fig. 7** Distribution of ZTD differences of BDS-only and GPS-only solutions with respect to the GPS/BDS combined solutions at stations XILA (top) and REUN (bottom) for day of year (DOY) = 60–90, i.e. about March 2014

description in Sect. 3.2 (post-processing to achieve highest quality for validation). We use the same elevation cutoff, prior tropospheric model, and mapping function as GNSS data processing. In order to avoid additional interpolation, only ZTD estimates at the common epochs from each ZTD series are taken into account for the comparisons. The ZTD biases resulting from the height difference between the phase center of GNSS antennas and the reference point of VLBI telescopes are corrected using the ‘troposphere ties’ method presented by Teke et al. (2011). It can be noticed that the ZTD of GPS/BDS combined solutions agrees quite well with the VLBI ZTD results with a small difference of about several millimeters. The ZTD of the single-system solutions, both GPS-only and BDS-only, also reveal good agreement with the VLBI ones. The differences between VLBI and BDS-only solutions present the largest values.

The ZTD differences of GPS-only, BDS-only, and GPS/BDS combined solutions with respect to the VLBI solutions for the two stations, ONS1 and WARK, are shown in Fig. 9, where the differences for the GPS/BDS combined solution are displayed by black symbols. In general the differences of the combined solution are smaller than 20.0 mm. The RMS values are 8.7 and 11.3 mm for the two stations, ONS1 and WARK, and the mean values of the differences are 2.0 and 2.2 mm, respectively. The ZTD differences for

GPS-only and BDS-only solutions are shown in the same figure indicated as red and blue symbols. We can see that the ZTD differences are the smallest for the combined solution, while the BDS-only differences are the largest. The RMS of BDS-only solution are 14.2 and 17.0 mm, and the RMS of GPS-only solution are 9.8 and 12.9 mm. Table 3 lists the statistics of the ZTD from BDS-only, GPS-only, and GPS/BDS combined solutions with respect to VLBI ZTD.

These results confirm the conclusion mentioned above that the real-time ZTD retrieved from BDS-only solution are also accurate enough (smaller than the threshold of 3 mm in PWV) and can be assimilated into the NWP models and applied in weather nowcasting. The combined solutions can improve the accuracy and reliability of real-time ZTD/PWV retrieval compared to the single-system solutions. Some outliers occurring in the GPS or BDS single-system solutions can be eliminated when the combined solutions are performed. Therefore, we can conclude that the BDS can contribute to real-time meteorological applications with slightly less accuracy than that of GPS, and more accurate and reliable ZTD/PWV estimates will be obtained, if the BDS observations are combined with the GPS observations in real-time PPP mode, about 1.3–1.8 mm in PWV.

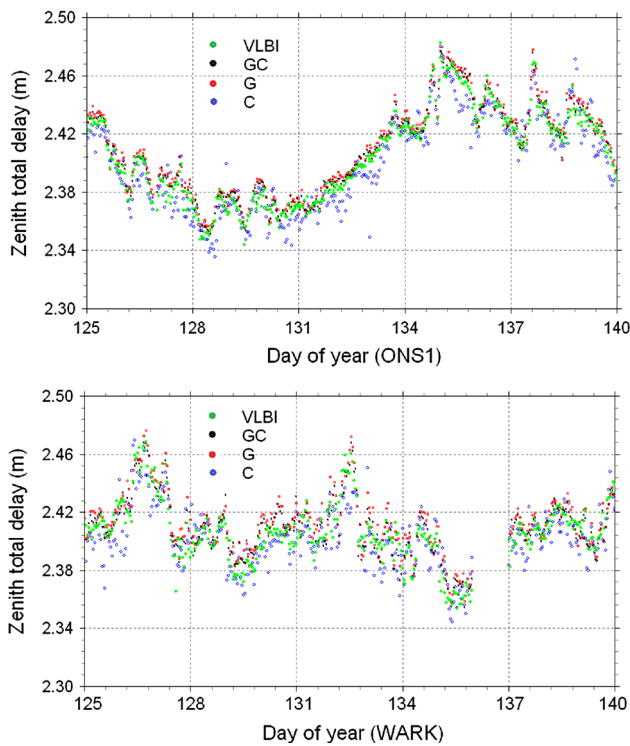


**Fig. 8** ZTD derived from GPS-only, BDS-only, GPS/BDS combined, and VLBI solutions at co-located stations ONS1/ONSALA60 (top) and WARK/WARK12M (bottom) from day of year (DOY) 125–140, i.e. 2014 May 6–20 (CONT14 campaign)

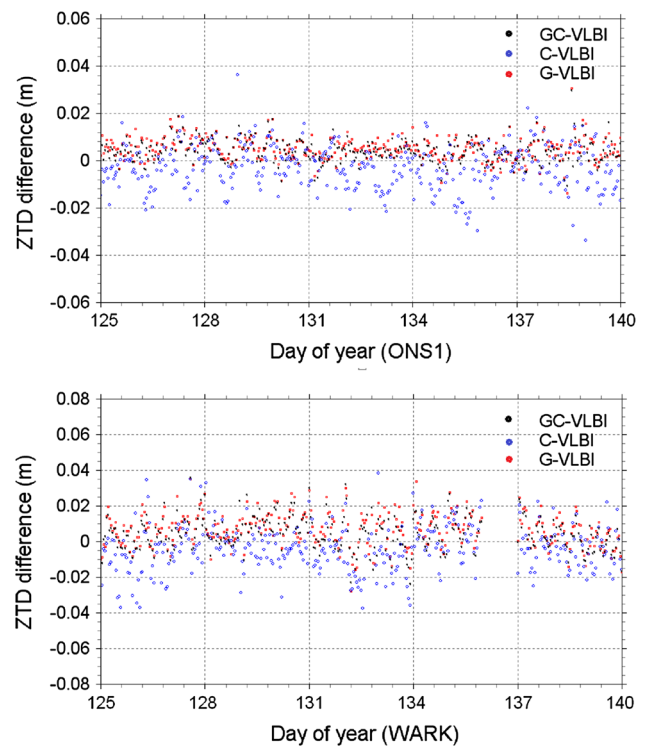


**Fig. 9** The ZTD differences of BDS-only, GPS-only, and GPS/BDS combined solutions with respect to the VLBI at ONS1/ONSALA60 (top) and WARK/WARK12M (bottom), from day of year (DOY) 125–140, i.e. 2014 May 6–20 (CONT14 campaign)

### 4.3 PWV validation of GNSS vs. radiosonde data

The PWV values derived from the real-time PPP analysis are validated using independent observations from radiosondes. Figure 10 shows the PWV results derived from the GPS/BDS combined real-time PPP solutions and nearby radiosonde solutions at stations ONS1 and WARK. The temporal resolutions of real-time PWV solutions derived from GNSS are 30 s while the radiosonde-retrieved PWV is sampled every 12 h. Accordingly, only PWV values at the common epochs are considered for the comparison. The GPS/BDS combined PWV agrees quite well with the radiosondes PWV with differences at the level of about few millimeters.

Figure 11 shows the RMS values of the PWV differences of the BDS-only, GPS-only, and GPS/BDS combined solutions with respect to the radiosonde solutions at five GNSS stations (CENT, SIGP, NNOR, ONS1, and WARK), where nearby radiosonde observations (distance <50 km) are

available. One can see that the differences of the combined solution vs. radiosondes are the smallest, while the BDS-only solution shows the largest differences. The RMS of the PWV differences are 1.5–1.8 mm for the GPS/BDS combined solution, 1.7–2.1 mm for the GPS-only solution, and 2.4–2.8 mm for the BDS-only solution. The corresponding statistics are summarized in Table 4. The PWV comparisons further confirm the aforementioned conclusion concerning the performance of BDS-derived real-time ZTD/PWV and the benefit of adding BDS to GPS-only processing. This confirms a potential benefit for real-time PWV retrieved from BDS in time-critical meteorological applications such as NWP nowcasting and severe weather event monitoring just like GPS. The combination of BDS-only and GPS-only PPP processing improves the performance concerning higher accuracy and robustness compared to the single-system solutions in meteorological applications.

**Table 3** Statistics of the ZTD from BDS-only, GPS-only, and GPS/BDS combined solutions w.r.t. VLBI ZTD

GNSS station	VLBI station	Bias (mm)			RMS (mm)		
		C-VLBI	G-VLBI	GC-VLBI	C-VLBI	G-VLBI	GC-VLBI
ONS1	ONSALA60	-3.0	2.9	2.0	14.2	9.8	8.7
WARK	WARK12M	-2.1	2.4	2.2	17.0	12.9	11.3

## 5 Conclusions and outlook

In this paper, we have developed a real-time ZTD/PWV retrieval algorithm combining GPS and BDS observations. The GPS and BDS data during the first half of the year 2014 from 40 BETN and MGEX stations were processed using the real-time PPP technique. The performance of the real-time ZTD/PWV derived from BDS was assessed and the contribu-

tion of adding BDS to the GPS-only approach for ZTD/PWV retrieval was carefully analyzed.

The results show that in general, the BDS-only ZTD derived from real-time PPP solution agree well with the GPS-only ZTD. The RMS values of the ZTD differences between BDS-only and GPS-only solutions are about 11–16 mm (about 2–3 mm in PWV), and the mean values of the differences are about a few millimeters (usually <1 mm in PWV). The agreement implies that the ZTD/PWV with BDS-only observations of the current constellation can also significantly contribute to weather nowcasting, although their accuracy is worse than the one of the current GPS-only solution (about 1.5 mm in PWV). Furthermore, some outliers, which appear in both single-system solutions, are eliminated in the combined solutions. The GPS/BDS combined ZTD are more robust and smoother than the single-system solutions, meaning that the addition of BDS to GPS observations can improve the quality of ZTD/PWV due to the increased number of satellites and the improved observation geometry.

The VLBI technique, as an independent validation for GNSS ZTD estimates, demonstrated a good agreement with the GPS/BDS combined solutions with a small difference of about several millimeters. The ZTD of the single-system solutions, both GPS-only and BDS-only, also reveal good agreement with the VLBI ones. The BDS-only solutions present the largest differences. We can conclude that the BDS can contribute to the real-time meteorological applications with slightly worse accuracy than that of GPS. As one of the most reliable measurements of water vapor, the radiosondes are employed for independent validation of the real-time PWV derived from GPS and BDS observations. The GPS/BDS combined PWV agree quite well with the PWV from radiosondes with differences at the level of few millimeters. The PWV of single-system solutions, both GPS and BDS, show good agreement with the ones from radiosondes. The differences of the GPS/BDS combined solutions

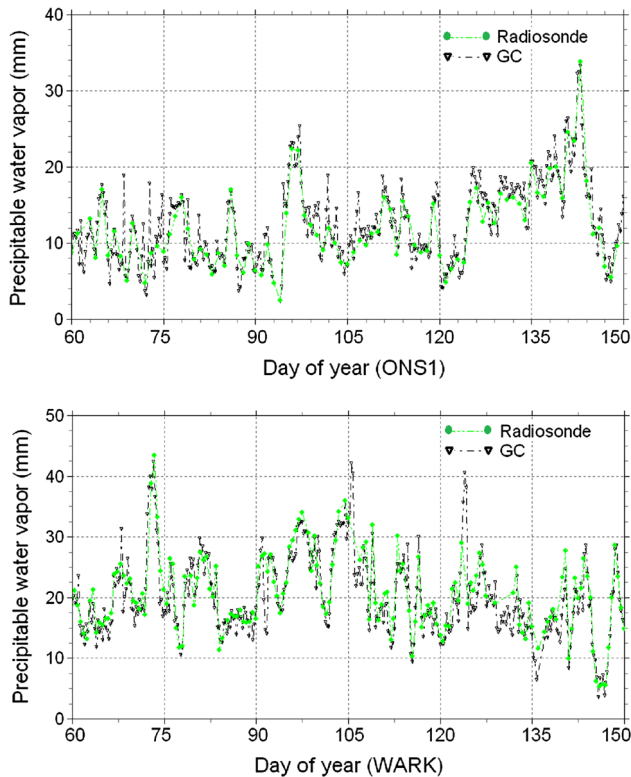


**Fig. 10** PWV derived from GPS/BDS combined real-time PPP and radiosonde solutions at stations ONS1 (top) and WARK (bottom) for day of year (DOY) 60–150 of 2014

**Fig. 11** RMS of PWV differences of BDS-only, GPS-only, and GPS/BDS combined solutions with respect to the radiosonde solutions

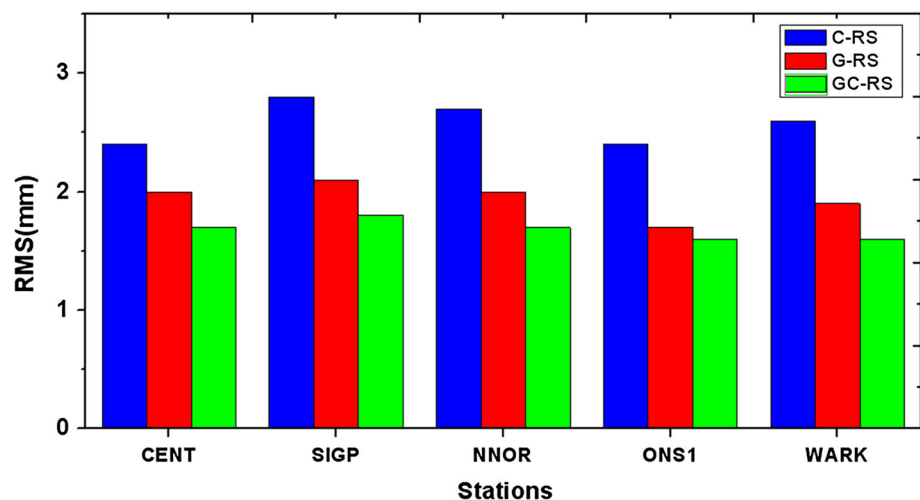


**Table 4** Statistics of the PWV differences of BDS-only, GPS-only, and GPS/BDS combined solutions with respect to the radiosonde solutions

Stations	Bias (mm)			RMS (mm)		
	C-RS	G-RS	GC-RS	C-RS	G-RS	GC-RS
CENT	0.1	-0.2	-0.1	2.4	2.0	1.7
SIGP	-0.2	0.1	0.0	2.8	2.1	1.8
NNOR	-0.3	-0.1	-0.1	2.7	2.0	1.7
ONS1	-0.5	0.4	0.2	2.4	1.7	1.6
WARK	-0.4	0.3	0.2	2.6	1.9	1.6

are the smallest, and those of the BDS-only solutions are the largest. The results further confirm the performance of BDS-derived real-time ZTD/PWV and the benefit of adding BDS to standard GPS-only processing for real-time ZTD/PWV retrieval, which can significantly contribute to time-critical meteorological applications such as NWP nowcasting and severe weather event monitoring.

Further studies related to comparisons and validations with respect to other techniques such as water vapor radiometer (WVR), numerical weather models (NWM) at a larger number of stations and over a longer time span will be in the focus of our future work. Furthermore, the performance of multiple combinations of GNSS systems, such as GPS, GLONASS, BDS, Galileo, and QZSS will also be investigated in future.

**Acknowledgments** We acknowledge IGS, MGEX, and BETN for providing the GPS and BDS data and IVS for providing the VLBI data. We also thank NOAA for the online provision of radiosonde data. One of the authors (C. Lu) is supported by the China Scholarship Council, which is gratefully acknowledged.

## References

- Askne J, Nordius H (1987) Estimation of tropospheric delay for microwaves from surface weather data. *Radio Sci* 22:379–386
- Bender M, Dick G, Wickert J, Ramatschi M, Ge M, Gendt G, Rothacher M, Raabe A, Tetzlaff G (2009) Estimates of the information provided by GPS slant data observed in Germany regarding tomographic applications. *J Geophys Res* 114:D06303. doi:10.1029/2008JD011008
- Böhm J, Niell A, Tregoning P, Schuh H (2006) Global Mapping Function (GMF): a new empirical mapping function based on numerical weather model data. *Geophys Res Lett* 33:L07304. doi:10.1029/2005GL025546
- Böhm J, Böhm S, Nilsson T, Pany A, Plank L, Spicakova H, Teke K, Schuh H (2012) The new Vienna VLBI software VieVS, Geodesy for Planet Earth. In: Proceedings of the 2009 IAG symp, Buenos Aires, International Association of Geodesy Symposia Series, vol 136, pp 1007–1011
- Bevis M, Businger S, Herring T, Rocken C, Anthes R, Ware R (1992) GPS meteorology: remote sensing of atmospheric water vapor using GPS. *J Geophys Res* 97:15787–15801
- Caissy M, Agrotis L, Weber G, Hernandez-Pajares M, Hugentobler U (2012) Coming soon: the International GNSS Real-Time Service. *GPS World*, vol 23(6), pp 52–58
- China Satellite Navigation Office (2012) BeiDou navigation satellite system signal in space interface control document. [http://gge.unb.ca/test/beidou\\_icd\\_english.pdf](http://gge.unb.ca/test/beidou_icd_english.pdf)
- Dow J, Neilan R, Rizos C (2009) The International GNSS Service in a changing landscape of Global Navigation Satellite Systems. *J Geod* 83:191–198. doi:10.1007/s00190-008-0300-3
- Davis J, Herring T, Shapiro I, Rogers A, Elgered G (1985) Geodesy by radio interferometry: effects of atmospheric modeling errors on estimates of baseline length. *Radio Sci* 20(6):1593–1607. doi:10.1029/RS020i006p01593
- Dousa J, Vaclavovic P (2014) Real-time zenith tropospheric delays in support of numerical weather prediction applications. *Adv Space Res* 53(9):1347–1358
- Elgered G, Plag H, van der Marel H, Barlag S, Nash J (eds) (2005) COST 716: exploitation of ground-based GPS for climate and numerical weather prediction applications, Final Report, European Community, EUR 21639, ISBN 92-898-0012-7
- Fang P, Bevis M, Bock Y, Gutman S, Wolfe D (1998) GPS meteorology: reducing systematic errors in geodetic estimates for zenith delay. *Geophys Res Lett* 25:3583–3586
- Gendt G, Dick G, Reigber C, Tomassini M, Liu Y, Ramatschi M (2004) Near real-time GPS water vapor monitoring for numerical weather prediction in Germany. *J Meteorol Soc Jpn* 82:361–370
- Gutman S, Sahn R, Benjamin G, Schwartz E, Holub L, Stewart Q, Smith L (2004) Rapid retrieval and assimilation of ground based GPS-Met observations at the NOAA forecast systems laboratory: impact on weather forecasts. *J Meteorol Soc Jpn* 82:351–360
- Ge M, Zhang H, Jia X, Song S, Wickert J (2012) What is achievable with the current COMPASS constellation? *GPS World* November, pp 29–34
- Haan S, Barlag S, Baltink H, Debie F (2004) Synergetic use of GPS water vapor and meteosat images for synoptic weather forecasting. *J Appl Meteorol* 43:514–518
- Heinkelmann R, Böhm J, Schuh H, Bolotin S, Engelhardt G, MacMillan D, Negusini M, Skurikhina E, Tesmer V, Titov O (2007) Combination of long time-series of troposphere zenith delays observed by VLBI. *J Geod* 81(6–8):483–501
- Kouba J (2009) A guide to using International GNSS Service (IGS) Products. <http://igsceb.jpl.nasa.gov/igsceb/resource/pubs/UsingIGSProductsVer21.pdf>
- Lagler K, Schindelegger M, Boehm J, Krásná H, Nilsson T (2013) GPT2: Empirical slant delay model for radio space geodetic techniques. *Geophys Res Lett* 40:1069–1073. doi:10.1002/grl.50288
- Li M, Li W, Shi C, Zhao Q, Su X, Qu L, Liu Z (2014a) Assessment of precipitable water vapor derived from ground-based BeiDou observations with Precise Point Positioning approach. *Adv Space Res* 55(1):150–162
- Li X, Zhang X, Ge M (2011) Regional reference network augmented precise point positioning for instantaneous ambiguity resolution. *J Geod* 85:151–158
- Li X, Ge M, Zhang H, Nischan T, Wickert J (2013a) The GFZ real-time GNSS precise positioning service system and its adaption for COMPASS. *Adv Space Res* 51(6):1008–1018
- Li X, Ge M, Zhang H, Wickert J (2013b) A method for improving uncalibrated phase delay estimation and ambiguity-fixing in real-time precise point positioning. *J Geod* 87(5):405–416
- Li X, Ge M, Zhang X, Zhang Y, Guo B, Wang R, Klotz J, Wickert J (2013c) Real-time high-rate co-seismic displacement from ambiguity-fixed precise point positioning: application to earthquake early warning. *Geophys Res Lett* 40(2):295–300. doi:10.1002/grl.50138
- Li X, Dick G, Ge M, Heise S, Wickert J, Bender M (2014b) Real-time GPS sensing of atmospheric water vapor: precise point positioning

- with orbit, clock and phase delay corrections. *Geophys Res Lett* 41(10):3615–3621
- Li X, Zhang X, Ren X, Fritsche M, Wickert J, Schuh H (2015) Precise positioning with current multi-constellation Global Navigation Satellite Systems: GPS, GLONASS, Galileo and BeiDou. *Sci Rep* 5:8328
- Montenbruck O, Steigenberger P, Khachikyan R, Weber G, Langley RB, Mervart L, Hugentobler U (2014) IGS-MGEX: preparing the ground for multi-constellation GNSS science. *Inside GNSS* 9(1):42–49
- Nilsson T, Elgered G (2008) Long-term trends in the atmospheric water vapor content estimated from ground-based GPS data. *J Geophys Res* 113:D19101. doi:10.1029/2008JD010110
- Nothnagel A (2009) Conventions on thermal expansion modeling of radio telescopes for geodetic and astrometric VLBI. *J Geod* 83:787–792. doi:10.1007/s00190-008-0284-z
- Ning T, Haas R, Elgered G, Willén U (2012) Multi-technique comparisons of 10 years of wet delay estimates on the west coast of Sweden. *J Geod* 86(7):565–575. doi:10.1007/s00190-011-0527-2
- Petit G, Luzum B (eds) (2010) IERS Conventions (2010), IERS Technical Note 36, Verlagdes Bundesamts für Kartographie und Geodäsie, Frankfurt am Main, Germany. <http://tai.bipm.org/iers/conv2010/>
- Ran C (2010) COMPASS Satellite System Development and Plan. In: Proceedings of The First China Satellite Navigation Conference, Beijing, China, 19–21 May 2010
- Rocken C, Van Hove T, Ware R (1997) Near real-time sensing of atmospheric water vapor. *Geophys Res Lett* 24:3221–3224
- Schuh H, Behrend D (2012) VLBI: a fascinating technique for geodesy and astrometry. *J Geodyn* 61:68–80. doi:10.1016/j.jog.2012.07.007
- Shi C, Zhao Q, Li M, Tang W, Hu Z, Lou Y, Zhang H, Niu X, Liu J (2012) Precise orbit determination of BeiDou Satellites with precise positioning. *Sci China Earth Sci* 55:1079–1086
- Saastamoinen J (1973) Contributions to the theory of atmospheric refraction—part II. Refraction corrections in satellite geodesy. *Bull Géod* 47(1):13–34. doi:10.1007/BF02522083
- Teke K, Boehm J, Nilsson T, Schuh H, Steigenberger P, Dach R, Heinkelmann R, Willis P, Haas R, Garcia-Espada S, Hobiger T, Ichikawa R, Shimizu S (2011) Multi-technique comparison of troposphere zenith delays and gradients during CONT08. *J Geod* 85:395–413. doi:10.1007/s00190-010-0434-y
- Wang J, Zhang L, Dai A (2005) Global estimates of water-vapor-weighted mean temperature of the atmosphere for GPS applications. *J Geophys Res* 110:D21101. doi:10.1029/2005JD006215
- Wang X, Wang X, Dai Z, Ke F, Cao Y, Wang F, Song L (2014) Tropospheric wet refractivity tomography based on the BeiDou Satellite System. *Adv Atmos Sci*. doi:10.1007/s00376-013-2311-0
- Xu A, Xu Z, Ge M, Xu X, Zhu H, Sui X (2013) Estimating zenith tropospheric delays from BeiDou navigation satellite system observations. *Sensors* 13:4514–4526
- Yang Y, Li J, Xu J, Tang J, Guo H, He H (2011) Contribution of the compass satellite navigation system to global PNT users. *Chin. Sci. Bull.* 56(26):2813–2819. doi:10.1007/s11434-001-4627-4
- Yuan Y, Zhang K, Rohm W, Choy S, Norman R, Wang C (2014) Real-time retrieval of precipitable water vapor from GPS precise point positioning. *J Geophys Res Atmos* 119:10044–10057
- Zumberge J, Heflin M, Jefferson D, Watkins M, Webb F (1997) Precise point positioning for the efficient and robust analysis of GPS data from large networks. *J Geophys Res* 102(B3):5005–5017